Pergamon

Int. J. Heat Mass Transfer. Vol. 40, No. 9, pp. 2019–2033, 1997

0017–9310/97 $17.00+0.00

PII: S0017–9310(96)00295–5

Theoretical and experimental studies of laminar mixed convection in water pipe flow with density inversion effect

G. J. HWANG and C. W. TSAI

Department of Power Mechanical Engineering, National Tsing Hua University, Hsinchu 30043, Taiwan, Republic of China

(*Received* 28 *March* 1996 *and in final form* 9 *August* 1996)

Abstract—The results of theoretical and experimental studies of the laminar mixed convection of water flow in a horizontal isothermally cooled pipe with the density inversion effect are presented. The theoretical solution uses the large Prandtl number assumption. The governing parameters of the flow and their ranges are the Rayleigh number Ra, $0 \leqslant Ra \leqslant 5 \times 10^7$, and the inlet temperature T_0, $5°C \leqslant T_0 \leqslant 18°C$, and wall temperature, $T_w = 0°C$. The effects of the density inversion on the flow and temperature fields and the Nusselt numbers are presented. The experiments were carried out by measuring the inlet, outlet and wall temperature. The secondary flow patterns were visualized by injecting a few drops of mercurochrome solution into the inlet tube. The measured and calculated heat transfer rate as well as photographs of the visualized secondary flow patterns and the numerically predicted flow patterns with density inversion effect are also presented.

1. INTRODUCTION

Extensive experimental [1–4] and theoretical [5–7] studies of the natural convection in a horizontal isothermal pipe have been performed in the past. Most of these studies are focused on fluids of constant thermal expansion coefficient. However, for the case of water near its freezing point, the use of constant thermal expansion coefficient is not justified, due to the fact that the density of water reaches a maximum value at about 4°C. After Merk [8], the problems of thermally driven convection of cold water have been studied by many researchers, not only because of their interesting features but also due to their environmental and engineering applications.

Heat transfer characteristics including the maximum density of water inside and around a horizontal cylinder were studied by Gilpin [9] and Saitoh [10], respectively. Transient natural convection of water in a horizontal pipe with a constant cooling rate and with a convective wall through 4°C were numerically examined by Cheng and Takeuchi [11], and Cheng *et al.* [12], respectively. All the calculations [9–12] used the temperature–density relationship developed by Fujii [13] to account for the variation of water thermal expansion coefficient. These investigations revealed that the heat transfer is strongly influenced by changing the flow pattern from a unicellular vortex into a counter-rotating bicellular form due to the density inversion at temperature near 4°C.

A number of studies have been reported in literature concerning the natural convection of cold water in a variety of cavities having different types of boundary conditions. Lankford and Bejan [14] conducted experiments in a vertical enclosure. The flow visualization is made using the thymol blue PH indicator technique. A combined experimental and theoretical investigation for the transient natural convection of water in a rectangular cavity was reported by Braga and Viskanta [15]. Photographs of flow visualization and predictions of the flow patterns were shown in their report. A helium–neon laser was used as the illumination source to trace the particle which is seeded in water. Numerical investigations for the transient heat transfer were performed by Robillard and Vasseur [16, 17]. The steady-state natural convection was studied by Lin and Nansteel [18] with a maximum Rayleigh number around 10^6. The density–temperature relationship of water adapted in [16] was developed by Moore and Weiss [19], in [17] was by Fujii [13], and in [18] was by Gebhart and Mollendorf [20], respectively. The findings in [16–18] showed that the anomalous density–temperature relationship may result in a multicellular flow pattern which significantly inhibits the cross-cavity heat transfer.

Several numerical researches concerned with natural convection water flow within a horizontal cylindrical annulus in a temperature range encompassing the maximum density have been published for concentric type by Nguyen *et al.* [21] and by Vasseur *et al.* [22] and for eccentric type by Ho and Lin [23]. They reported that the appearance of bicellular flow patterns occurs in the annulus, and that the average

NOMENCLATURE

a tube radius [m]
c specific heat of liquid [J kg^{-1} K^{-1}]
D tube diameter $= 2a$ [m]
f body force
$F(\theta)$ equation (5)
F_0 equation (6)
F_i $i = 1, 2$ and 3, coefficients of equation (5)
g gravitational acceleration [ms^{-2}]
Gr Grashof number $= g\beta_0(T_0 - T_w)a^3/\nu^2$ based on tube radius
h heat transfer coefficient
k fluid thermal conductivity [W m^{-1} K^{-1}]
$\dot{m}$ mass flow rate [g s^{-1}]
Nu Nusselt number $= hD/k$
$\bar{p}, p$ main-stream and cross-stream pressures, respectively [Nm m^{-2}]
$\bar{P}, P$ dimensionless main-stream and cross-stream pressures, respectively
Pr Prandtl number, ν/α
$q, \bar{q}$ local and total heat transfer rate, respectively, $\bar{q} = 2a\int_0^z \int_0^\pi q \, d\phi \, dz$ [W]
q^* dimensionless heat transfer rate, $q^* = \bar{q}/\pi a^2 w_0 \rho_0 c(T_0 - T_w)$
r, ϕ cylindrical coordinates [m, rad]
R, ϕ dimensionless cylindrical coordinates, $R = r/a$
Ra Rayleigh numbers $= PrGr$
Re Reynolds number $= w_0 D/\nu$
T temperature [°C]
T_i $i = 1, 2 \ldots 9$, temperature indicated by ith thermocouple [°C]
T_{md} maximum density temperature, $T_{md} = 4$°C
w_0 mean flow velocity at inlet [m s^{-1}]
u, v, w velocity components [m s^{-1}]
U, V, W dimensionless velocity components
z, Z dimensional and dimensionless axial distances, $Z = z/a \, Pr \, Re$.

Greek symbols
α fluid thermal diffusivity [m^2 s^{-1}]
β thermal expansion coefficient [K^{-1}]
β_i $i = 1, 2, 3$ and 4, constants of equation (1)
γ inversion parameter, $\gamma = (T_{md} - T_w)/(T_0 - T_w)$
ν kinematic viscosity [m^2 s^{-1}]
θ dimensionless temperature, $\theta = (T - T_w)/(T_0 - T_w)$
ρ water density [kg m^{-3}]
ρ_f water density at 0°C [kg m^{-3}]
σ standard deviation of wall temperature [°C]
ψ dimensionless stream function
ζ dimensionless vorticity
ΔT $T_0 - T_w$
∇^2 dimensionless Laplace operator

$$= \frac{1}{R}\frac{\partial}{\partial R}\left(R\frac{\partial}{\partial R}\right) + \frac{1}{R^2}\frac{\partial^2}{\partial \phi^2}.$$

Subscripts
a average
b bulk
e outlet
f freezing point or fully developed state
i, j nodal points
m mean
o inlet
r film
w wall.

Superscript
k the kth iteration.

heat transfer coefficient exhibited a minimum value when the two counter-rotating eddies were of approximately the same size.

All these studies [21–23] mentioned above concerned only two-dimensional problems without the main flow. The mixed convection flow in a horizontal isothermal tube is three-dimensional and is hard to analyze theoretically. In practical engineering applications, the mixed convection flows are frequently encountered. For example, the water flow in a chiller. Recently, Hwang and Lai [7] successfully solved the laminar mixed convective heat transfer in a horizontal isothermal tube for Rayleigh numbers up to 10^8. But the fluid density concerned in [7] is a linear temperature–density relationship. So far, theoretical and experimental investigations on the laminar mixed convective flow for water through the maximum density have not been found yet. The attempt of this study is to solve both experimentally and numerically the laminar mixed convection heat transfer of water flow in a horizontal isothermally cooled pipe with the density inversion effect.

2. THEORETICAL ANALYSIS

2.1. *The temperature–density relationship*

According to Fujii [13], the density–temperature relationship for water as depicted in Fig. 1 can be approximated by the following equation with an error

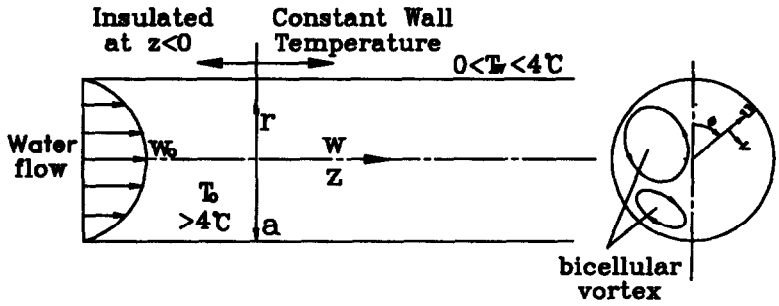

Fig. 1. Physical model and coordinate system.

of less than one unit at the last digit of the tabulated data [11]:

$$1/\rho = (1/\rho_f)(1+\beta_1 T+\beta_2 T^2+\beta_3 T^3+\beta_4 T^4) \quad (1)$$

where $\rho_f = 0.9998396$ (g cm^{-3}) is the water density at freezing point 0°C,

$$\beta_1 = -0.678964520\times 10^{-4} \quad (°C^{-1}),$$

$$\beta_2 = 0.907294338\times 10^{-5} \quad (°C^{-2}),$$

$$\beta_3 = -0.964568125\times 10^{-7} \quad (°C^{-3}),$$

$$\beta_4 = 0.873702983\times 10^{-9} \quad (°C^{-4}).$$

The thermal expansion coefficient β is evaluated as

$$\beta = -\frac{1}{\rho}\frac{\partial \rho}{\partial T}\bigg|_p.$$

In the present study, if the inlet temperature of 12°C and wall temperature of 0°C are posed. The value of thermal expansion coefficient β will be decreased when the water is cooled and a negative value of β will be observed if $T < 4$°C. This phenomenon will greatly affect the strength of the secondary flow.

2.2. *Formulation of the problem*

The following assumptions are made in the theoretical analysis:

(1) The flow is laminar and incompressible.

(2) The fluid thermophysical properties are constant except density in the r- and ϕ- momentum equations.

(3) Axial conduction and viscous dissipation are negligible.

(4) The volume flow rate is constant, even though the water density is changing along the flow direction due to the continuous cooling.

Since the cooling of water temperature from 20°C to 0°C causes a density variation of only 0.18%, the assumption for constant volume flow rate is justified. It is also noted that the variation of water thermal diffusivity α in the temperature range of 20°C to 0°C is only 7.6%. The change of water kinematic viscosity ν from 20°C to 0°C is $\pm 20\%$ based on 10°C. This may have significant effect on the Grashof number Gr which is proportional to $1/\nu^2$. Fortunately, the increase in kinematic viscosity due to cooling of the flow assures the validity of large Prandtl number assumption. The Grashof number can be combined with the Prandtl number, and the Rayleigh number Ra becomes the governing parameter as will be seen in equation (4). A discussion on the evaluation of Ra will be made in the present study.

Without loss of the generality, the pressure distribution in the flow can be expressed as $\bar{p}(z)+p(r,\phi,z)$ where the first term indicates the pressure distribution for the fully developed flow, and the second term is the pressure deviation from the fully developed one.

For facilitating the analysis one introduced the following dimensionless transformations

$$R = \frac{r}{a};\ Z = \frac{z}{aRePr};\ W = \frac{w}{2w_0};\ \theta = \frac{T-T_w}{T_0-T_w}$$

$$U = \frac{ua}{Grv};\ V = \frac{va}{Grv};\ P = \frac{p}{\rho_0\beta_0 g(T_0-T_w)a};$$

$$\bar{P} = \frac{\bar{p}}{\rho_0 Pr(2w_0)^2}$$

where $Re = 2w_0 a/\nu$ is the Reynolds number and $Gr = \beta_0 g(T_0-T_w)a^3/\nu^2$ is the Grashof number. The r- and ϕ-direction characteristic velocity $\beta_0 g(T_0-T_w)a^2/\nu$ and characteristic pressure $\rho_0\beta_0 g(T_0-T_w)a$ can be obtained readily by equalizing the magnitudes of the pressure, viscous and buoyancy terms. The dimensionless axial coordinate and pressure include the Prandtl number, because of the effects of thermal diffusivity are considered in these two quantities.

The final governing equations in dimensionless form for the computation are:

$$\nabla^2\zeta = -\left[\frac{\partial F(\theta)}{\partial R}\sin\phi + \frac{1}{R}\frac{\partial F(\theta)}{\partial \phi}\cos\phi\right] \quad (2)$$

$$\nabla^2\psi = \zeta \quad (3)$$

$$W_f\frac{\partial\theta}{\partial Z} = \left[\frac{1}{R}\frac{\partial}{\partial R}\left(R\frac{\partial\theta}{\partial R}\right)+\frac{1}{R^2}\frac{\partial^2\theta}{\partial\phi^2}\right] - Ra\left[U\frac{\partial\theta}{\partial R}+\frac{V}{R}\frac{\partial\theta}{\partial\phi}\right] \quad (4)$$

where

$$U = \frac{1}{R}\frac{\partial \psi}{\partial \phi} \quad V = -\frac{\partial \psi}{\partial R}$$

and

$$F(\theta) = (\beta_w/\beta_0)(\theta + F_1\theta^2 + F_2\theta^3 + F_3\theta^4) \quad (5)$$

$$F_1 = (\beta_2 + 3\beta_3 T_w + 6\beta_4 T_w^2)\Delta T/F_0$$

$$F_2 = (\beta_3 + 4\beta_4 T_w)\Delta T^2/F_0$$

$$F_3 = \beta_4 \Delta T^3/F_0$$

$$\Delta T = T_0 - T_w$$

$$F_0 = \beta_1 + 2\beta_2 T_w + 3\beta_3 T_w^2 + 4\beta T_w^3. \quad (6)$$

β_0 and β_w indicate the thermal expansion coefficient of water at the inlet and wall, respectively. The buoyancy force due to density change based on reference of the wall temperature is expressed as $(\rho - \rho_w)/\rho = -(T_0 - T_w)\beta_0 F(\theta)$.

The value of $F(\theta)$ determines the direction of the buoyancy force in the flow. It is worthy to mention that a dimensionless inversion parameter $\gamma = (T_{md} - T_w)/(T_0 - T_w)$ presented in Gebhart and Mollendorf [20] is an indication of the direction of the buoyancy force. Note that for values of γ in the range $0 < \gamma < 1$, the flow encompasses the maximum density temperature T_{md}. In the present study, $5°C \leqslant T_0 \leqslant 18°C$ and $T_w = 0°C$ correspond to $0.22 < \gamma < 0.8$.

Equations (2)–(4) are subjected to the following boundary conditions:

$$\psi(1, \phi, Z) = \frac{\partial \psi(1,\phi,Z)}{\partial R} = 0 \quad 0 \leqslant \phi \leqslant \pi \quad Z \geqslant 0$$

$$\psi(R, \phi, Z) = \zeta(R, \phi, Z) = 0$$

$$0 \leqslant R \leqslant 1 \quad \phi = 0 \text{ and } \pi \quad Z \geqslant 0$$

$$\theta(R, \phi, 0) = 1 \quad 0 \leqslant R < 1 \quad 0 \leqslant \phi \leqslant \pi \quad (7)$$

$$\frac{\partial \theta(R, \phi, Z)}{\partial \phi} = 0 \quad 0 \leqslant R \leqslant 1 \quad \phi = 0 \text{ and } \pi \quad Z \geqslant 0$$

$$\theta(1, \phi, Z) = 0 \quad 0 \leqslant \phi \leqslant \pi \quad Z \geqslant 0.$$

It is noted that the symmetric condition on the center plane may be reasonable due to the slow natural convection flow.

The variation of heat transfer coefficient is significantly affected by the natural convection. The heat transfer coefficients can be obtained by considering either the wall temperature gradient or the axial temperature gradient.

$$Nu_1 = \frac{hD}{k} = \frac{2}{\pi\theta_b}\int_0^\pi -\left.\frac{\partial\theta}{\partial R}\right|_{R=1} d\phi \quad (8)$$

or

$$Nu_2 = \frac{-1}{2\pi\theta_b}\int_0^\pi\int_0^1 \frac{\partial\theta}{\partial Z} W_f R \, dR \, d\phi \quad (9)$$

where

$$\theta_b = \frac{2}{\pi}\int_0^\pi\int_0^1 \theta W_f R \, dR \, d\phi$$

is the dimensionless bulk temperature. The accuracy of the numerical predictions can be assessed by the degree of agreement of Nu_1 and Nu_2. The dimensionless heat transfer rate q^* from the liquid to the ambient at a dimensionless axial position Z can be calculated as

$$q^* = \frac{\bar{q}}{\pi a^2 w_0 \rho_0 c(T_0 - T_w)} = \frac{4}{\pi}\int_0^z\int_0^\pi -\left.\frac{\partial\theta}{\partial R}\right|_{R=1} d\phi \, dZ \quad (10)$$

where

$$\bar{q} = 2a\int_0^z\int_0^\pi q \, d\phi \, dz \text{ and } q = -k\left.\frac{\partial T}{\partial r}\right|_{r=a}$$

are the overall and local heat transfer rate, respectively. By considering the overall temperature drop between the inlet and the outlet conditions, thus the dimensionless heat transfer rate q^* can be written as $q^* = (T_0 - T_e)/(T_0 - T_w)$.

For understanding the effect of the density inversion on the buoyancy force, three mean thermal expansion coefficients are evaluated for a fixed Z plane as

$$\beta_m = \frac{2}{\pi}\int_0^\pi\int_0^1 \beta_{i,j} W_f R \, dR \, d\phi \quad (11)$$

is the mean thermal expansion coefficent, and

$$\beta_b = -\frac{1}{\rho}\left.\frac{\partial\rho}{\partial T}\right|_p \text{ evaluated at } T_b \quad (12)$$

is the bulk thermal expansion coefficient, and

$$f_m = \frac{2g}{\pi}\int_0^\pi\int_0^1 [(\rho_{i,j} - \rho_w)/\rho_{i,j}] W_f R \, dR \, d\phi \quad (13)$$

is the mean buoyancy force [11] where the buoyancy force is based on reference state at the wall temperature.

The difference between β_m and β_b provides an evaluation of the drastical change of the temperature field. And the value of f_m shows the net body force of the fluid flow by integration of the buoyancy force on each Z plane.

3. NUMERICAL SOLUTION

In this study, the governing equations are discretized by using the weighting function scheme [24] to enhance the stability and accuracy of the numerical computation. The P-method scheme [25] dealing with the axial derivative in energy equation is adapted here to increase the numerical accuracy and enlarge the step size. Energy equation in R and ϕ directions is

Table 1. Numerical experiments of grid sizes

	$T_0 = 18°C$, $Ra = 5 \times 10^7$					
$M \times N$	99×31		91×31†		91×21	
Z	Nu_1	Nu_2	Nu_1	Nu_2	Nu_1	Nu_2
1×10^{-4}	63.44	64.18	63.92	64.79	64.04	65.38
1.03×10^{-3}	59.49	60.35	59.95	60.98	60.11	61.06
1.15×10^{-2}	35.87	35.99	34.95	34.75	33.44	33.40
1.09×10^{-1}	15.84	15.81	15.71	15.67	15.78	15.75
0.5	4.19	4.19	4.19	4.18	4.21	4.20
	$T_0 = 12°C$, $Ra = 10^7$					
$M \times N$	91×31		81×31†		81×21	
Z	Nu_1	Nu_2	Nu_1	Nu_2	Nu_1	Nu_2
1×10^{-4}	41.25	41.71	41.44	41.94	41.42	43.02
1.03×10^{-3}	38.16	38.29	38.34	38.54	38.42	38.60
1.15×10^{-2}	27.62	27.56	27.51	27.49	26.12	25.66
1.09×10^{-1}	14.97	14.94	14.95	14.93	14.99	14.97
0.5	4.16	4.15	4.16	4.15	4.18	4.17
	$T_0 = 5°C$, $Ra = 10^6$					
$M \times N$	71×31		61×31†		61×21	
Z	Nu_1	Nu_2	Nu_1	Nu_2	Nu_1	Nu_2
1×10^{-4}	28.20	28.34	28.11	28.33	28.11	28.33
1.03×10^{-3}	18.22	18.25	18.22	18.27	18.32	18.55
1.15×10^{-2}	24.39	24.43	24.46	24.55	25.02	25.09
1.09×10^{-1}	14.05	14.03	14.02	14.00	13.99	13.97
0.5	4.11	4.11	4.11	4.11	4.12	4.12

† Number of grids used in this study.

of elliptic type and is solved by the SIS algorithm developed by Lee [26] for the temperature distribution. A relaxation factor of 1.5 is used in this study. The convergence criterion for temperature fields is set as $|(T_{i,j}^{k+1} - T_{i,j}^k)/T_{i,j}^k| \leqslant 10^{-4}$. The singularity at the origin of the polar coordinates is avoided by using a Cartesian form of the governing equation there. A boundary–vorticity method developed by Hwang and Cheng [27] is used to get the vorticity and the stream functions of the flow. The iteration of ζ and ψ at each axial step is terminated when the stream function satisfies the criterion $|(\psi_{i,j}^{k+1} - \psi_{i,j}^k)/\psi_{i,j}^{k+1}| \leqslant 5 \times 10^{-4}$. The numerical solution procedure used here is given in Hwang and Lai [7], a detailed description will not be repeated here. The finite-difference grid sizes are uniform in both the r- and ϕ- directions. Typical grid independence study is listed in Table 1. The number of grids for various Ra and T_0 used in the present study are those marked with †. The difference between the solutions obtained with grid no. and their corresponding finer grids is small and can be neglected. Number of grids in r- and ϕ- directions is 91×31 for $Ra = 5 \times 10^7$, 81×31 for $Ra = 10^7$, 71×31 for $Ra = 5 \times 10^6$, 61×31 for $Ra = 10^6$, 51×31 for $Ra = 10^5$, 41×31 for $Ra = 10^4$, and 31×31 for $Ra < 10^4$. The axial step sizes are varied from $\Delta Z = 10^{-8}$ near the entrance to 10^{-4} at the downstream for all value of Rayleigh numbers [7]. All the computations are terminated at $Z = 0.8$ in the present study.

4. EXPERIMENTAL STUDY

As pictured schematically in Fig. 2(A), the experiments were carried out in a closed loop water flow cooling system. This system was assembled by four major parts including a constant temperature water reservoir, a constant head tank, a cooling system and a test section. Distilled water was stored in the constant temperature water reservoir and pumped up to the constant head tank. The constant head tank provided a desired flow rate to the test section where the water flow is cooled by the coolant supplied from the coolant bath. The water in the test section then flowed back to the constant temperature water reservoir.

The constant temperature water reservoir provided water flow with desired temperature. Its cooling capacity is 9000 Btu h^{-1} and a pump with 1 hp was used to deliver the water flow. A PID controller was built in to control the water temperature at the outlet of the reservoir. The range of the water temperature can be regulated from 0°C to 35°C within an error of ± 0.1°C. It delivered water flow up to the constant head tank and received water from the overflow tubing and from the outlet of the test section.

The constant head tank was made of plastic plates. The vertical distance between the overflow plate and the outlet of the tank near the bottom was 35 cm which gave a sufficient flow rate for the experiment. A thermocouple (T-type coded as T_0) was located at the bottom of the tank (near the inlet of the test section) to indicate the inlet bulk water temperature. A dye injection device was connected to the water piping to inject the dye into the water flow. Convergent and divergent plexiglass heads were connected to the inlet and outlet of the test section, respectively. A filter was installed at each end of the head to smooth the flow. A mixing chamber was used to homogenize the outlet water temperature and a thermocouple (T-type coded as T_e) was plugged in the mixing chamber for the indication of the outlet bulk water temperature. A control valve was connected to the exit of the mixing chamber for regulating the water flow rate.

The cooling system pumps the coolant to cool the test section. The coolant was a solution of 75% distilled water and 25% ethyl alcohol. The solution was stored and cooled in a 1.5 ton refrigerator and pumped to the annular space of the test section. The freezing point of the solution is below -12°C which is low enough to perform the experiment. The piping system of the coolant and the exterior of the test section had been well insulated to reduce the thermal loading of the cooling system.

As shown in Fig. 2(b), the test section was made of copper tube with 3.8 cm i.d. and 4.14 cm o.d. and was jacketed by plexiglass with 7 cm i.d. and 8 cm o.d. The cooling length of the test section is 81.1 cm. A light-guided ring with 7 mm in thickness was made of plexiglass and was embedded between copper tubes to lighten the cross-section for flow visualization from the outlet. The location of the light-guided ring was

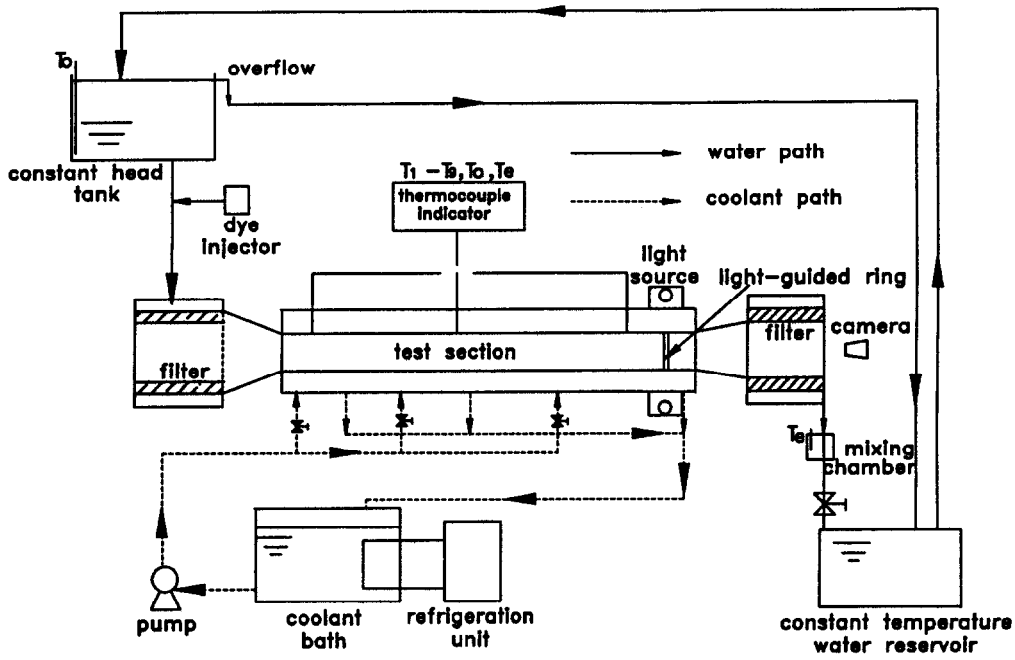

(A) Experimental System

Fig. 2(A). Schematic of experimental apparatus.

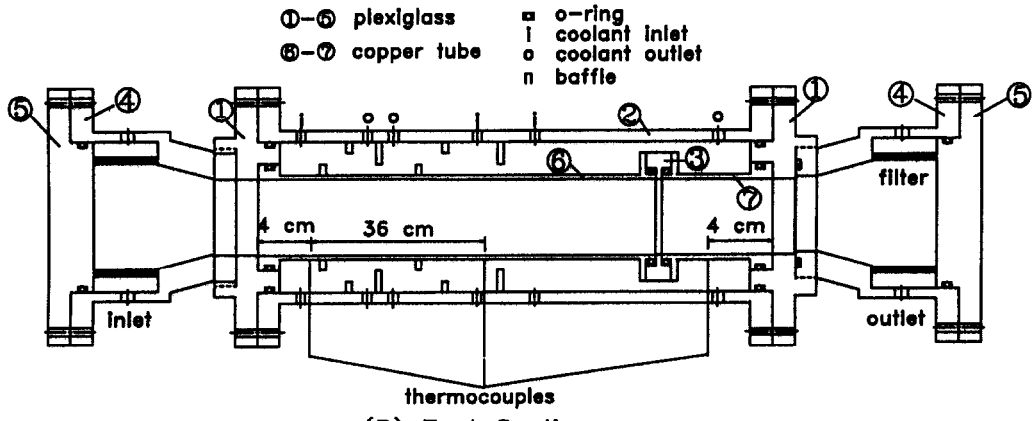

(B) Test Section

Fig. 2(B). Test section.

76 cm away from the inlet of the test section. A ring type lamp was mounted around the light-guided ring to provide the light source. Several baffles were installed to enhance the heat transfer rate for cooling of the test section. Nine thermocouples (T-type coded as T_1–T_9) were uniformly welded at three positions on the copper tube wall to measure the wall temperatures. At each position, three thermocouples were welded equi-peripherally around the copper tube wall with 120° apart. The locations of the thermocouples is shown in Fig. 2(B).

In order to achieve the constant wall temperature conditions, three pairs of inlet and outlet of coolant pipings were designed for individually controlling the coolant flow rate. Each inlet and outlet of the coolant piping has four coolant passages equi-peripherally located around the outer tube of the test section. The wall temperature distribution could be regulated by the adjustment of the coolant flow rate at each passage. Thus the wall temperature distribution could be properly tuned to meet the uniform condition.

To visualize the secondary flow patterns, the water flow was seeded with a small amount of mercurochrome solution when the system reaches its steady state condition. The mercurochrome solution is diluted with distilled water of a ratio of 30 : 1 to make sure the flow pattern is well exhibited and not disturbed. The light emitted from the ring type lamp illuminates the seeded solution for picture taking. Photographs of the flow patterns were taken using

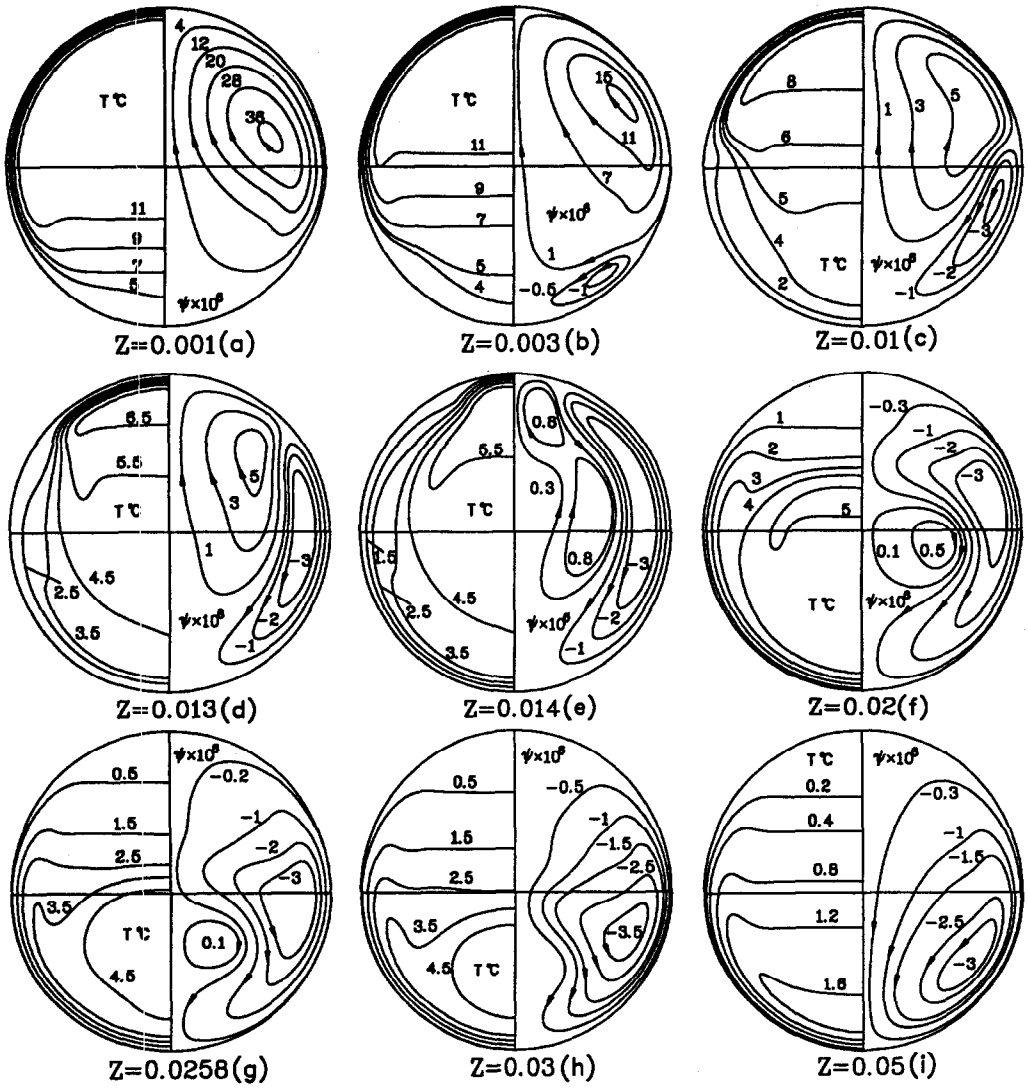

Fig. 3. Streamline patterns and isotherms for $T_0 = 12°C$, $T_w = 0°C$ and $Ra = 10^7$.

Fuji ISO 400 film, exposure time 0.5 s and aperture of 3.5.

5. RESULTS AND DISCUSSION

5.1. *Theoretical results*

For studying the secondary flow inversion process due to the maximum density, the streamlines and isotherms for inlet water temperature $T_0 = 12°C$, wall temperature $T_w = 0°C$, and Rayleigh number $Ra = 10^7$ are plotted in Fig. 3(a)–(i). The inversion parameter γ in this case is equal to 1/3. The flow patterns are drawn on the right half of the cross-section and isotherms are on the left half. At the initial stage of cooling $Z = 0.001$ [Fig. 3(a)], a vortex with a large downward velocity near the side wall transports the cooled water to the bottom part of the pipe, and then moves upward. Thus it is seen that the isotherms in the lower region are sparsely spaced and thermally stratified, and a large temperature gradient near the upper wall appears. As the flow moves downstream, continuous cooling of the fluid produces a small region with $T < 4°C$ near the bottom part. In this region, the density of the water generates a flow reversal. The flow region with a pair of counter-rotating vortices is similar to those reported in refs. [11, 12]. The upper and lower vortices meet at a point near the wall and form a cold spot, and a low local wall heat flux appears. The location of cold spot shifts from the bottom $\phi = \pi$ toward the upper portion $\phi = 0$ as Z increases. At about $Z = 0.013$, the bottom-counter-clockwise vortex grows up and competes with the upper one. At $Z = 0.014$, a pair of approximately equal size counter-rotating vortices exists. Vasseur *et al.* [22] reported that the Nusselt Number Nu will decrease to a minimum value when this pair of counter-rotating vortices are with approximately the same size. A similar vortex formation was reported by Saitoh and Hirose [28] for the convection of flow surrounding a horizontal ice cylinder and by Vasseur *et*

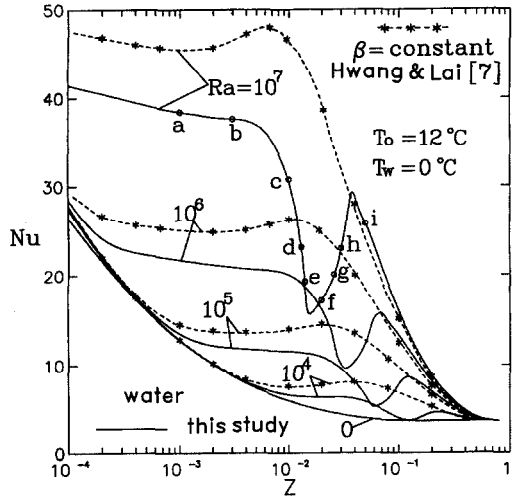

Fig. 4. Comparison of theoretical Nusselt number between density inversion case and constant β case.

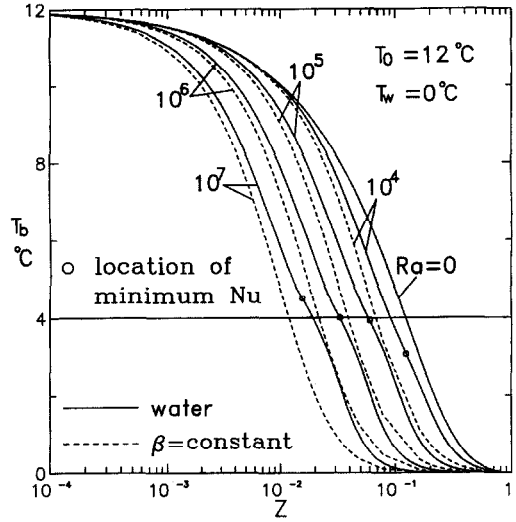

Fig. 5(a). Theoretical bulk temperature for $T_0 = 12°C$, $T_w = 0°C$ and $Ra = 0$–10^7.

al. [22] for the convection within a horizontal cylindrical annulus. As fluid flows further downstream at $Z = 0.03$, the strength of the upper vortex decreases and finally the counter-clockwise vortex overwhelms the original one and the inversion process is totally completed. At $Z = 0.05$, the cooled water is transported to the top, where the minimum local wall heat flux exists near $\phi = 0$.

The variations of local Nusselt number Nu with the dimensionless axial length Z for inlet water temperature $T_0 = 12°C$ and various Rayleigh numbers Ra with inversion parameter $\gamma = 1/3$ are plotted in Fig. 4. The Nusselt numbers with constant thermal expansion coefficient β as shown in Hwang and Lai [7] are also plotted for comparison. It is seen that the calculated water data are much lower than that for constant β case. The prediction of the smaller Nu for water flow is due to mainly the occurrence of the maximum density in this temperature range 0–12°C and also the decreased β along the flow direction. The corresponding locations (a)–(i) in Fig. 3 are also marked on the water curve for $Ra = 10^7$. With the effect of density inversion, the Nu decreases along the axial direction to a minimum value then moves up to a maximum one. And then the Nu decays monotonically to the asympotatic value of 3.66. The generation of two pairs of counter-rotating vortices inhibits the heat transfer rate. The locations of the minimum Nu occur at the axial position where two pairs of counter-rotating vortices are approximately equal size, as shown in Figs. 3(e) and (f) for $Z = 0.014$–0.02. This confirms the statement of Vasseur *et al.* [22]. As the Rayleigh number Ra increases, the decrease in Nu for water from that of constant thermal expansion coefficient β is more pronounced and the location for the minimum Nu moves to the upstream direction due to earlier formation of the counter-rotating vortices.

The variations of the bulk fluid temperature T_b and

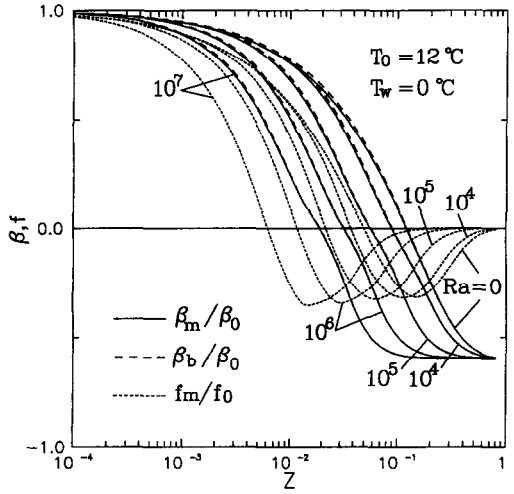

Fig. 5(b). Variations of β_m/β_0, β_b/β_0 and f_m/f_m vs dimensionless axial distance Z for $T_0 = 12°C$, $T_w = 0°C$ and $Ra = 0$–10^7.

the normalized coefficients of buoyancy force terms β_m/β_0, β_b/β_0 and f_m/f_0 with the dimensionless axial length Z for $T_0 \leqslant 12°C$ and inversion parameter $\gamma = 1/3$ are plotted in Figs 5(a) and (b), respectively. The predictions of the bulk fluid temperature T_b for fluids with constant thermal expansion coefficient β are also shown. For $Ra > 0$, the bulk fluid temperatures of the water flow is higher than those of β = constant due to the lower heat transfer rate. It is interesting to see that T_b is around 4°C at the location of minimum Nu. From equations (11)–(13), β_m is the mean thermal expansion coefficient, β_b is the bulk thermal expansion coefficient, and f_m is the mean buoyancy force term. It shows that both β_m/β_0 and β_b/β_0 with a small difference decrease monotonically with the axial position. This is probably due to the thin thermal boundary layer caused by the large Prandtl number of water flow. The temperature distribution

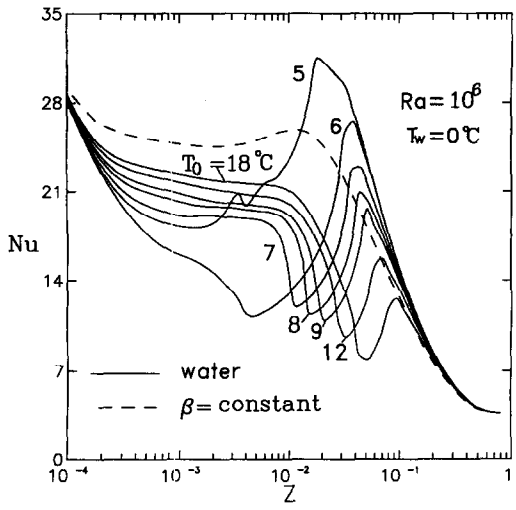

Fig. 6. Effect of inlet temperature on Nusselt number for $Ra = 10^6$ and $T_w = 0°C$.

of the flow is flat and the temperature in most of the region across the pipe is close to the bulk fluid temperature. This yields approximately the same value of β_m and β_b. The ratio of f_m/f_0 indicating the ratio of buoyancy force, decreases from unity to a negative minimum value then goes up asympotatically to zero. It also shows that the mean buoyancy force f_m reaches asympotatic zero earlier for larger Ra than for smaller Ra. This is due to the rapid decrease of the bulk fluid temperature. It is noted that the position of minimum values f_m/f_0 is almost identical to the locations of minimum Nusselt number Nu.

Figure 6 exhibits the variations of local Nusselt number Nu with the dimensionless axial position Z for various inlet water temperature T_0 from 5°C to 18°C for $Ra = 10^6$. The range of inversion parameter is $0.22 \leqslant \gamma \leqslant 0.8$. Theoretical predictions of Nu for the case of β = constant are also shown. For water flow with $Ra = 10^6$, tremendous effect of inlet temperature T_0 on the Nu has been revealed. At the initial stage of cooling, the Nusselt number Nu decreases with the decrease in T_0 and the deviation from that of β = constant is more pronounced when a pair of counter rotating vortices with approximately equal size establishes. The location of the minimum Nu shifts toward upstream as T_0 decreases, indicating the earlier establishment of the inversion process. It is seen that the trend of the variations of the Nu for the cases of $T_0 = 5°C$ is apparently different from those of above 6°C and is thus worthy to study in detail the heat transfer characteristics with the inlet water temperature T_0 close to 4°C. From Fig. 6, during the late period of the decay in the Nu and discrepancy between the water case and β = constant case increases with the decrease in T_0.

Due to the maximum density at 4°C, one may expect different flow characteristics for the inlet water temperature close to 4°C. From Fig. 6, one observes that the trend of the variations of the Nu for $T_0 = 5°C$ is much different from that of T_0 above 6°C. Figure 7 shows the streamline patterns and isotherms for the inlet water temperature $T_0 = 5°C$ and inversion parameter $\gamma = 0.8$ for $Ra = 10^6$. From Fig. 7 for $T_0 = 5°C$, the streamline patterns and isotherms exhibits a totally different flow field as compared with Fig. 3. During the initial stages of cooling before $Z = 0.0002$, a main counter-clockwise vortex forms causing a downward velocity near the center core, and the isotherms are nearly concentrically distributed. The cooler water near the wall will be carried directly into the core region and the isotherms at the top wall become distorted and sparsely spaced as cooling proceeds. This kind of flow pattern is completely contrary to that of Fig. 3. A second vortex with smaller size is generated beneath the center core at $Z = 0.0015$ and then a tricellular vortex is observed at $Z = 0.002$. Later, the upper smaller vortex disappear owing to the cold water keeping pulling downward and the inner vortex grows increasingly and pulls upward at $Z = 0.004$. One can see a sudden little decrease in the Nu contemporarily as shown in Fig. 6 at $Z = 0.004$, revealing that a pair of counter-rotating vortices with approximate size exists. After this point, the clockwise vortex starts to decay rapidly. As cooling further proceeds, the smaller vortex near the center core disappears and the main vortex also starts to decrease due to the decrease in the bulk fluid temperature. This peculiar flow pattern for $T_0 = 5°C$ causes significant different feature of the Nusselt number Nu.

5.2. *Experimental results*

To run an experiment, the system of the experimental facility operates for at least 3 h to reach the steady state condition. The inlet water temperature T_0 is controlled by the constant temperature water reservoir. The wall temperature of the test section is adjusted by the settings of the cooling system and regulated by the coolant flow rate. Measurements of wall temperature distribution were made with nine thermocouples coded as T_1–T_9. The mean wall temperature T_w was then calculated as the average value of these nine data

$$T_w = \frac{1}{9}\sum_{i=1}^{9} T_i$$

and was used in the numerical predictions. The degree of uniformity of wall temperature can be shown by the standard deviation of wall temperature σ which is defined as

$$\sigma = \sqrt{\sum_{i=1}^{9}(T_i - T_w)^2/9}.$$

In this study, three different series of experiments were conducted by covering wide ranges of the inlet and wall temperatures as well as the flow rate. In series (I), 20 runs were performed to measure the dimensionless heat transfer rate without density inver-

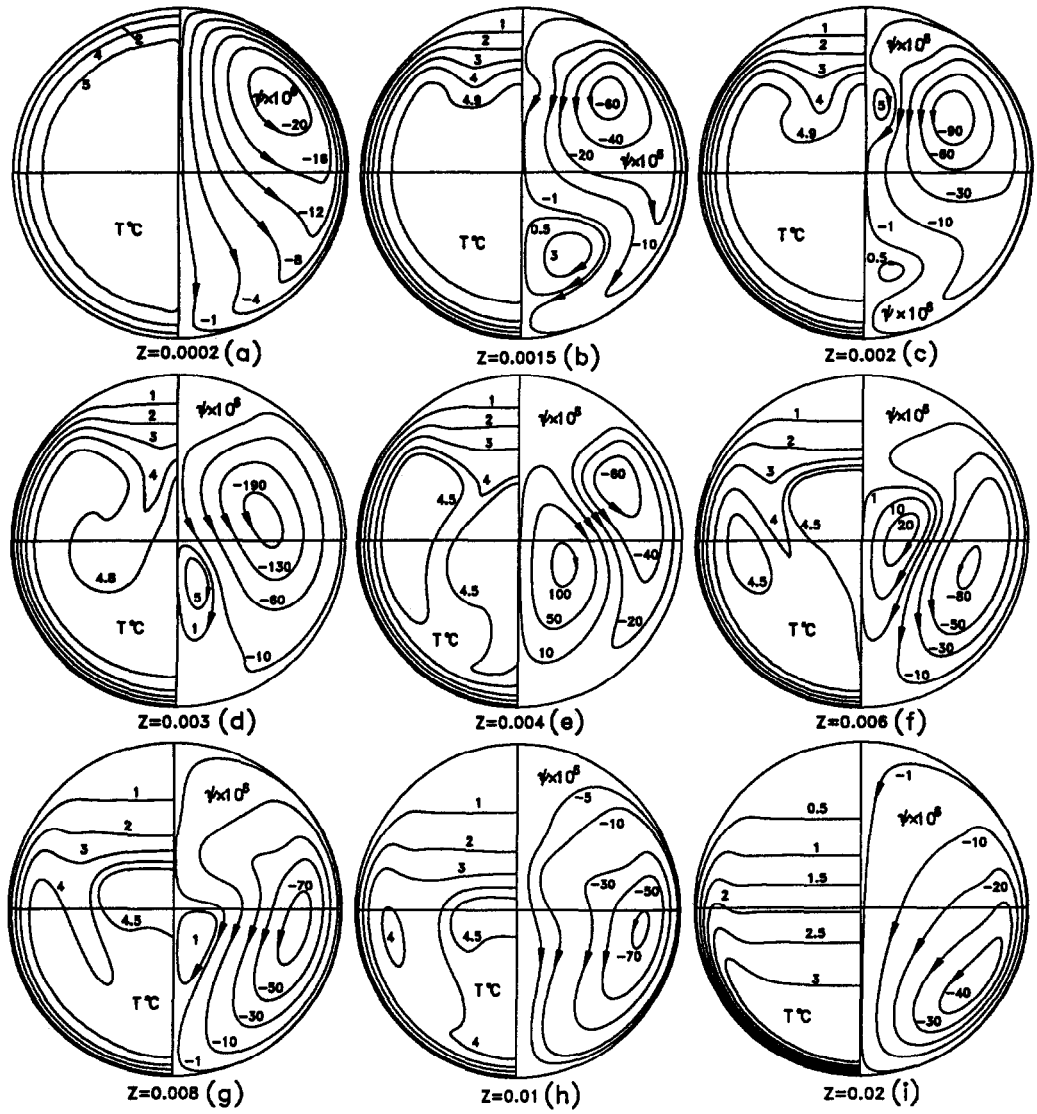

Fig. 7. Steamline patterns and isotherms for $T_0 = 5°C$, $T_w = 0°C$ and $Ra = 10^6$.

sion for providing a comparison with the previous results of other researchers. In series (II), 20 runs were performed to measure the dimensionless heat transfer rate for exhibiting the effect of density inversion on the heat transfer characteristic. In series (III), 10 runs were performed to visualize the secondary flow patterns with the density inversion effect. The experimental data for these 50 runs are shown in Tables 2 and 3. It is noted that in all these experiments no ice formation was observed even though there were some temperature readings slightly below 0°C.

Data reduction and correlation are the major tasks of exploring the experimental results. For cases without density inversion, the fluid properties β, ν and α used in calculating the Rayleigh number Ra and dimensionless axial length Z were evaluated based on the film temperatures $T_r = (T_a + T_w)/2$ [4], where $T_a = (T_0 + T_e)/2$ is the average temperature, T_0 is the inlet water temperature, T_e is the outlet water temperature, T_w is the wall temperature. For cases with density inversion, the thermal expansion coefficient β was evaluated at the average temperature T_a but not the film temperature T_r to give a better correlation as shown in Fig. 8. The reasons are given in the following statements. For the case without density inversion, boundary layer type secondary flow is observed near the pipe wall. The film temperature has been proven successfully in the literature for describing the heat transfer characteristic in the natural convection flow. It is believed that this can be also extended to the present mixed convection flow. For the case with density inversion, the flow region in the cross-section is much more mixed by the extra one pair of counter rotating vortices than the boundary layer type secondary flow for the case without density inversion. Therefore, the average temperature may give a closer estimation of the thermal expansion coefficient for this case.

Table 2. Data for heat transfer measurement

Run no.	T_0 [°C]	T_e [°C]	T_w [°C]	σ [°C]	Ra [$\times 10^{-5}$]	[q^*]	Z [$\times 10^2$]	$\dot{m}$ [g s^{-1}]
(A) $T_w > 4$°C								
1	24.3	20.5	7.0	0.15	9.4	0.220	0.419	42.6
2	31.0	23.2	8.6	0.29	15.06	0.348	0.706	25.6
3	31.0	21.4	8.2	0.34	13.9	0.421	0.919	19.6
4	31.2	19.1	7.8	0.33	12.6	0.517	1.199	15.0
5	33.2	20.2	13.9	0.29	12.54	0.674	1.934	9.4
6	31.0	14.4	7.7	0.31	9.67	0.713	2.294	7.8
7	31.1	17.7	12.8	0.20	10	0.732	2.699	6.8
8	39.5	16.1	8.9	0.47	16	0.764	3.122	5.8
9	35.9	15.3	11.8	0.23	12	0.855	4.533	4.0
10	36.0	13.2	10.1	0.25	11.3	0.880	5.011	3.6
11	20.6	17.5	6.0	0.18	6.19	0.212	0.527	33.8
12	20.5	16.8	6.1	0.15	5.83	0.257	0.711	25.0
13	19.7	15.0	5.9	0.16	4.81	0.341	0.889	20.0
14	21.6	15.7	6.9	0.19	5.76	0.401	1.068	16.7
15	20.5	15.0	9.1	0.13	4.6	0.483	1.484	12.0
16	22.8	14.3	8.6	0.19	5.39	0.599	2.035	8.8
17	26.1	13.0	7.8	0.22	6.4	0.716	3.029	5.9
18	25.9	11.4	7.7	0.23	5.65	0.797	4.284	4.2
19	31.1	24.9	23.7	0.06	6.03	0.838	4.889	3.8
20	31.1	25.7	25.2	0.05	4.74	0.915	6.396	2.9
(B) $T_w \approx 0$°C								
1	20.4	16.3	0.2	0.24	12.43	0.203	0.521	33.8
2	24.1	18.0	0.2	0.38	17	0.255	0.640	27.7
3	24.4	15.0	−0.1	0.38	14.82	0.384	0.929	19.0
4	24.4	10.8	0.2	0.39	11.29	0.562	1.584	11.1
5	27.3	10.1	0.2	0.44	12.99	0.635	2.123	8.3
6	26.8	7.6	0.2	0.39	10.7	0.722	3.479	5.1
7	29.1	7.1	0.1	0.39	12.1	0.759	3.911	4.5
8	27.8	6.0	0.1	0.31	10.32	0.787	4.932	3.6
9	27.9	5.2	0.0	0.28	9.9	0.814	6.176	2.8
10	30.7	5.3	0.2	0.34	11.89	0.833	6.252	2.8
11	15.2	12.1	0.2	0.17	6.2	0.207	0.582	30.0
12	15.7	11.0	0.1	0.18	5.9	0.302	0.877	19.9
13	16.0	9.4	0.3	0.19	5.17	0.420	1.299	13.4
14	17.2	8.0	0.1	0.22	5.14	0.538	1.978	8.8
15	17.6	8.8	0.2	0.22	5.71	0.506	2.284	7.6
16	17.9	6.9	0.1	0.22	4.94	0.618	2.961	5.9
17	18.6	6.2	0.1	0.19	4.94	0.670	3.755	4.6
18	20.2	5.8	0.2	0.25	5.51	0.720	4.429	3.9
19	19.1	5.0	0	0.18	4.6	0.738	5.431	3.2
20	21.1	5.1	0.1	0.18	5.65	0.762	6.405	2.7

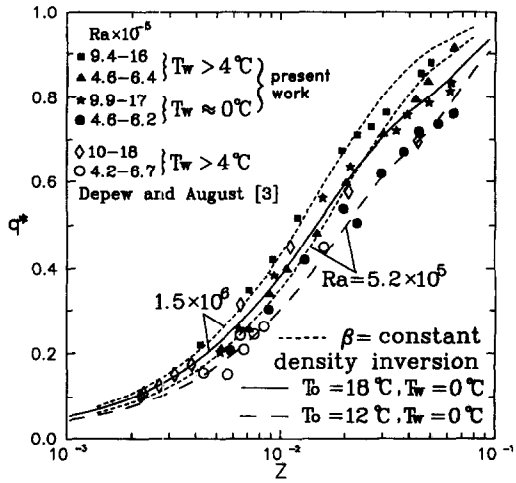

Fig. 8. Comparison of experimental and theoretical heat transfer rates.

The calculation of the experimental uncertainty in a result Ψ could be expressed as [29]

$$\delta\Psi = \left\{\left[\frac{\partial\Psi}{\partial x_1}\delta x_1\right]^2 + \cdots + \left[\frac{\partial\Psi}{\partial x_n}\delta x_n\right]^2\right\}^{1/2}. \quad (14)$$

The symbol $\partial\Psi/\partial x$ stands for the partial derivative of the result Ψ with respect to the variable x. And δx based on 95% confidence is evaluated as

$$\delta x = \{(B_{inst})^2 + (2\sigma_{run})^2\}^{1/2} \quad (15)$$

where B_{inst} is the fixed error arising from the instrument itself and σ_{run} is the standard deviation of the running trials. We are concerned with the result of q^* vs Z. Recall that $q^* = (T_0 - T_e)/(T_0 - T_w)$ and $Z = z\alpha/2a^2w_0$; the experimental uncertainty for q^* and Z could be calculated as

$$\delta q^* = q^*\left\{\left[\frac{\delta T_0}{(T_0 - T_e)}(1-q^*)\right]^2 + \left[\frac{\delta T_w}{(T_0 - T_e)}q^*\right]^2 + \left[\frac{\delta T_e}{(T_0 - T_e)}\right]^2\right\}^{1/2} \quad (16)$$

$$\delta Z = Z\left\{\left[\frac{\delta z}{z}\right]^2 + \left[\frac{\delta\alpha}{\alpha}\right]^2 + \left[\frac{2\delta a}{a}\right]^2 + \left[\frac{\delta w_0}{w_0}\right]^2\right\}^{1/2}. \quad (17)$$

The percentage of experimental uncertainty of q^* and Z was calculated as $\delta q^*/q^*$ and $\delta Z/Z$, respectively. Most of the value of $\delta q^*/q^*$ lie within 3% and may reach maximum value of 5%. For $\delta Z/Z$, the values are less than 2%.

Figure 8 presents the dimensionless heat transfer rate q^* with dimensionless axial length Z for both experimental and predicted results. Experimental data of Depew and August [3] are also shown in the same plot. The dimensionless heat transfer rate q^* is calculated as $q^* = (T_0 - T_e)/(T_0 - T_w)$. From Fig. 8, it is seen that the agreement between experimental results and theoretical prediction is excellent. The decrease in the dimensionless heat transfer rate q^* for density inversion case is conspicuous due to the density inversion effect. Experimental work of Depew and August [3] for $T_w > 4$°C shows close consistency with this study for $Z \leqslant 10^{-2}$. While for $Z > 10^{-2}$, a large discrepancy of q^* between this study and Depew and August [3] is observed. This discrepancy may be due to the average temperature T_a instead of film tempera-

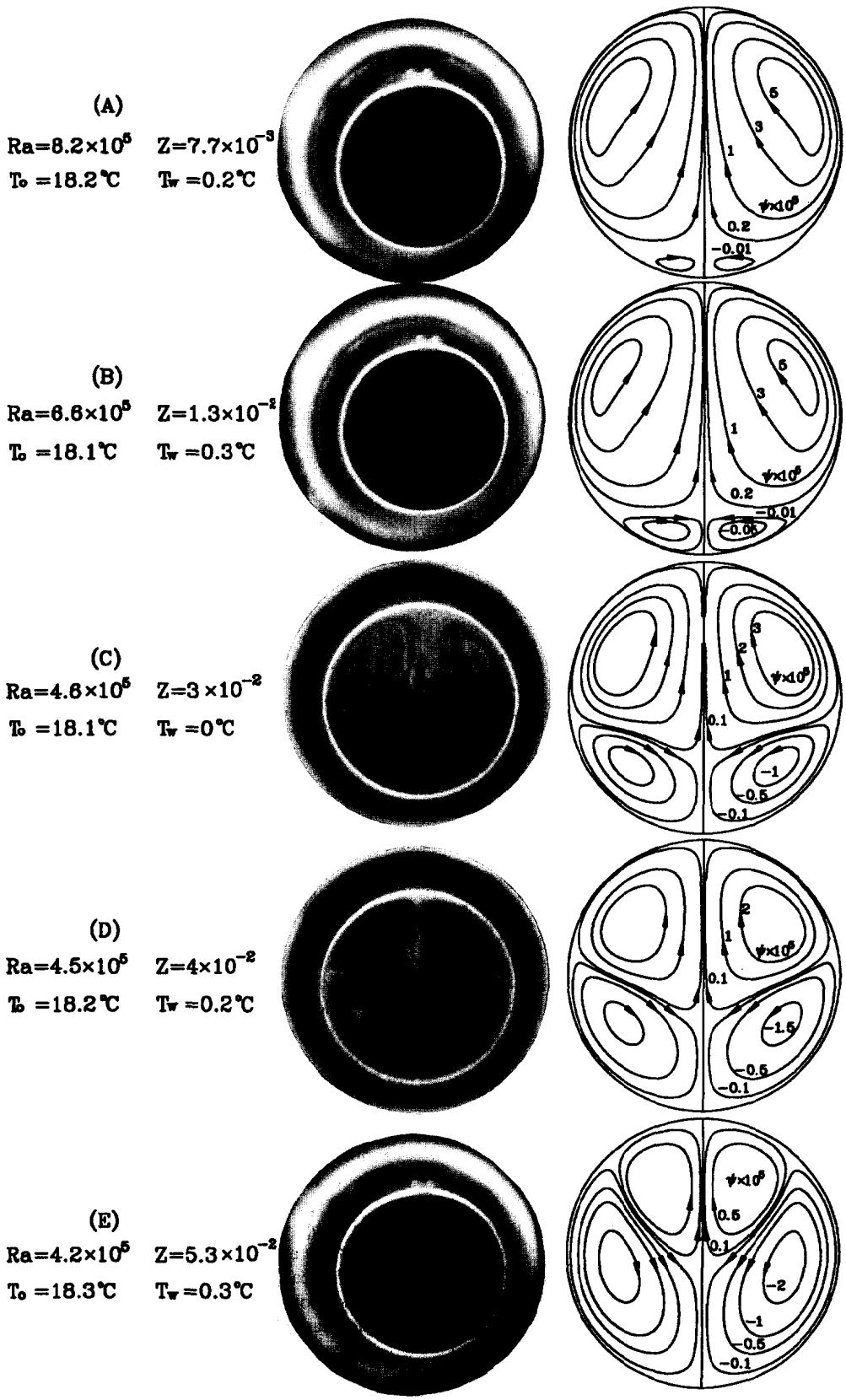

Fig. 9. Photographs of flow pattern and predicted streamlines for $T_0 \approx 18°C$ and $T_w \approx 0°C$.

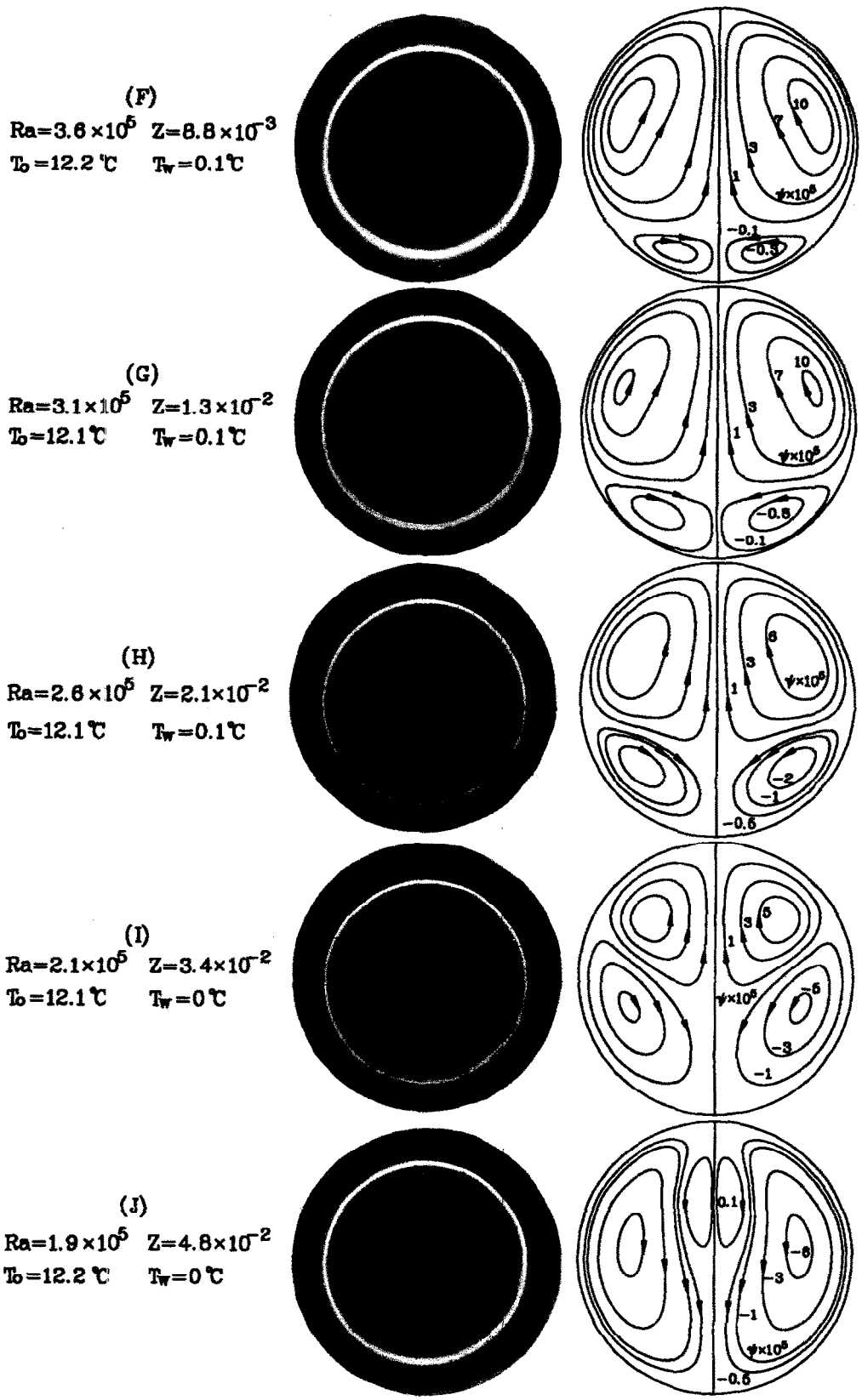

Fig. 10. Photographs of flow pattern and predicted streamlines for $T_0 \approx 12°C$ and $T_w \approx 0°C$.

Table 3. Data for flow visualization

Run no.	T_0 [°C]	T_c [°C]	T_w [°C]	σ [°C]	Ra [$\times 10^{-5}$]	[q^*]	Z [$\times 10^2$]	$\dot{m}$ [g s^{-1}]	Run no.	T_0 [°C]	T_c [°C]	T_w [°C]	σ [°C]	Ra [$\times 10^{-5}$]	[q^*]	Z [$\times 10^2$]	$\dot{m}$ [g s^{-1}]
A	18.2	12.5	0.2	0.24	8.2	0.317	0.77	19.9	F	12.2	9.7	0.1	0.14	3.6	0.207	0.88	18.5
B	18.1	10.0	0.3	0.27	6.6	0.455	1.3	13.2	G	12.1	8.6	0.1	0.14	3.1	0.29	1.3	12.3
C	18.1	6.0	0.0	0.25	4.6	0.669	3.0	5.4	H	12.1	7.2	0.1	0.13	2.6	0.408	2.1	7.7
D	18.2	5.7	0.2	0.23	4.5	0.694	4.0	4.1	I	12.1	5.6	0	0.12	2.1	0.537	3.4	4.7
E	18.3	5.0	0.3	0.17	4.2	0.739	5.3	3.1	J	12.1	4.9	0	0.1	1.9	0.598	4.8	3.4

ture T_r being used for the evaluation of thermophysical properties in their experiment without density inversion.

In order to examine the effect of density inversion on the flow fields, 10 runs of experiment for flow visualization were conducted. By controlling the inlet water temperature and the wall temperature, and adjusting the water flow rate, a sequential evaluation of flow patterns can be observed. Photographs of flow patterns as well as the calculated flow fields for $T_0 \approx 18°C$ and $T_w \approx 0°C$ are presented in Fig. 9. The experimental and predicted flow fields are quite similar. The visualized flow structure along the vertical center plane are different from that from the numerical solution. These discrepancies may be due to the simplified linear secondary flow model in the numerical calculation with the assumptions of large Pr and small Gr. Similar results are shown in Fig. 10 for $T_0 \approx 12°C$ and $T_w \approx 0°C$. Due to the density inversion effect, two pairs of counter rotating vortices coexist in all experiments for flow visualizations (A)–(J). It can be clearly seen that the sequential evolution of two pairs counter-rotating vortices.

6. CONCLUSIONS

The study of mixed convection of water flow in an isothermal horizontal pipe have been carried out both experimentally and numerically. The density–temperature relationship of water around 4°C uses the one developed by Fujii [13]. The theoretical solution uses large Prandtl number assumption [7]. The problem then is shown to depend on the Rayleigh number Ra, inlet water temperature T_0 and wall temperature T_w. The predicted results are obtained for $0 \leqslant Ra \leqslant 5 \times 10^7$, $5°C \leqslant T_0 \leqslant 18°C$ and $T_w = 0°C$. The numerical and experimental results obtained in this study provide further insight into the inversion process which is unique to water possessing a maximum density at 4°C. An analysis of the flow patterns and heat transfer characteristics shows that:

(1) The density inversion has a significant effect on the laminar mixed convection heat transfer for water flow. This is particularly true in cases where two counter rotating vortices of approximate size coexist. Under this circumstance, the Nusselt number Nu is considerably reduced. This phenomenon is more pronounced with the decrease in the inlet water temperature T_0 for each Rayleigh number Ra and with the increase in Rayleigh number Ra for each inlet water temperature T_0.

(2) The computed results show that the original vortex is clockwise and the second vortex generated by density inversion during cooling process started from the bottom sidewall for $T_0 \geqslant 6°C$. While for $T_0 \leqslant 5°C$, the inversion process is totally contrary. And a tricellular vortex is observed.

(3) The predicted and measured heat transfer rate as well as the flow patterns are in good agreement. Experimental results show a distinguished decrease in heat transfer rate with the density inversion effect. The secondary flow patterns were successfully visualized by using the mercurochrome solution. In all experiments for flow visualization, two pairs of counter rotating vortices exhibited in the test section which were caused by the density inversion.

(4) It is believed that the inversion process due to the maximum density effect of water may have some influence on the results of laminar pipe flow solidification when using water as the working medium.

REFERENCES

1. D. Q. Kern and D. F. Othmer, Effect of free convection on viscous heat transfer in horizontal tubes, *A.I.Ch.E. Jl* **39,** 517–555 (1943).
2. D. R. Oliver, The effect of natural convection on viscous-flow heat transfer in horizontal tubes, *Chem. Engng Sci.* **17,** 335–350 (1962)
3. C. A. Depew and S. E. August, Heat transfer due to combined free and forced convection in a horizontal and isothermal tube, *J. Heat Transfer* **93,** 380–384 (1971).
4. S. M. Mocros and A. E. Bergles, Experimental investigation of combined forced and free laminar convection in horizontal tubes, *J. Heat Transfer* **97,** 212–219 (1975).
5. Jenn-Wuu Ou and K. C. Cheng, Natural convection effects on Graetz problem in horizontal isothermal tubes, *Int. J. Heat Mass Transfer* **20,** 953–960 (1977).
6. M. Hishida, Y. Nagano and M. S. Montesclaros, Combined forced and free convection in the entrance region of an isothermally heated horizontal pipe, *J. Heat Transfer* **104,** 153–159 (1982).
7. G. J. Hwang and H. C. Lai, Laminar convective heat transfer in a horizontal isothermal tube for high Rayleigh numbers, *Int. J. Heat Mass Transfer* **37,** 1631–1640 (1994).
8. H. J. Merk, The influence of melting and anomalous expansion on the thermal convection in laminar boundary layers, *Appl. Sci. Res.* **4,** 435–452 (1954).
9. R. R. Gilpin, Cooling of a horizontal cylinder of water through its maximum density point at 4°C, *Int. J. Heat Mass Transfer* **18,** 1307–1315 (1975).

10. T. Saitoh, Natural convection heat transfer from a horizontal ice cylinder, *Appl. Sci. Res.* **32,** 429–451 (1976).
11. K. C. Cheng and M. Takeuchi, Transient natural convection of water in a horizontal pipe with constant cooling rate through 4°C, *J. Heat Transfer* **98C,** 581–587 (1976).
12. K. C. Cheng, M. Takeuchi, and R. R. Gilpin, Transient natural convection in horizontal water pipes with maximum density effect and supercooling, *Numer. Heat Transfer* **1,** 101–115 (1978).
13. T. Fujii, Fundamentals of free convection heat transfer, *Progress in Heat Transfer Engineering*, Yokendo, Tokyo, Vol. 3, pp. 66 (1974).
14. K. E. Lankford and A. Bejan, Natural convection in a vertical enclosure filled with water near 4°C, *J. Heat Transfer* **108,** 755–763 (1986).
15. S. L. Braga and R. Viskanta, Transient natural convection of water near its density extremum in a rectangular cavity, *Int. J. Heat Mass Transfer* **35,** 861–875 (1992).
16. L. Robillard and P. Vasseur, Transient natural convection heat transfer of water with maximum density effect and supercooling, *J. Heat Transfer* **103,** 528–534 (1981).
17. L. Robillard and P. Vasseur, Convective response of a mass of water near 4°C to a constant cooling rate applied on its boundaries, *J. Fluid Mech.* **118,** 123–141 (1982).
18. D. S. Lin and M. W. Nansteel, Natural convection heat transfer in a square enclosure containing water near its density maximum, *Int. J. Heat Mass Transfer* **30,** 2319–2329 (1987).
19. D. R. Moore and N. O. Weiss, Nonlinear penetrative convection, *J. Fluid Mech.* **61,** 553–581 (1973).
20. B. Gebhort and J. C. Mollendorf, Buoyancy-induced flows in water under conditions in which density extrema may arise, *J. Fluid Mech.* **89,** 673–707 (1978).
21. T. H. Nguyen, P. Vasseur and L. Robillard, Natural convection between horizontal concentric cylinders with density inversion of water for low Rayleigh numbers, *Int. J. Heat Mass Transfer* **25,** 1559–1568 (1982).
22. P. Vasseur, L. Robillard and B. C. Shekar, Natural convection heat transfer of water within a horizontal cylindrical annulus with density inversion effects, *J. Heat Transfer* **105,** 117–123 (1983).
23. C. J. Ho and Y. H. Lin, Natural convection heat transfer of cold water within an eccentric horizontal cylindrical annulus. *J. Heat Transfer* **110,** 894–900 (1988).
24. S. L. Lee, Weighting function scheme and its application on multidirectional conservation equations, *Int. J. Heat Mass Transfer* **32,** 2065–2073 (1989).
25. S. L. Lee, A new numerical formulation for parabolic differential equations under the consideration of large time steps, *Int. J. Numer. Meth. Engng* **26,** 1541–1549 (1988).
26. S. L. Lee, A strongly implicit solver for two-dimensional elliptic differential equations, *Numer. Heat Transfer B* **16,** 161–178 (1989).
27. G. J. Hwang and K. C. Cheng, Boundary vorticity method for convective heat transfer with secondary flow application to the combined free and forced laminar convection in horizontal tubes, *Proceedings of the 4th International Heat Transfer Conference*, Versailles, Paris, Vol. 4, Paper no. NC3.5 (1970).
28. T. Saitoh and K. Hirose, Thermal instability of natural convection flow over a horizontal ice cylinder encompassing a maximum density point, *J. Heat Transfer* **102,** 261–267 (1980).
29. R. J. Moffat, Describing the uncertainties in experimental results, *Exp. Thermal Fluid Sci.* **1,** 3–17 (1988).